Two-Species Chemotaxis Systems on Weighted Graphs: Asymptotic Behavior and Numerical Simulations

GEORGES CHAMOUN
Faculty of Engineering (ESIB)
Saint Joseph University of Beirut
B.P 11-514 Riad El Solh, Beyrouth 1107 2050
LEBANON

Abstract: This paper presents a rigorous mathematical analysis of a two-species chemotaxis-competition model on weighted networks, incorporating nonlinear degenerate chemotactic sensitivities and volume-filling effects. The aim is to understand long-term population dynamics in networked environments. Using a Lyapunov functional approach, we characterize the asymptotic behavior of solutions. Under weak competition, coexistence occurs with exponential convergence, while strong competition leads to the extinction of one species and algebraic convergence to a segregated state. These theoretical results are validated through numerical simulations that highlight the effects of competition parameters, network topology, and initial conditions. The proposed numerical scheme demonstrates convergence with exponential or algebraic decay of relative errors, in agreement with the analytical results. This study highlights the role of network structure in shaping chemotaxis-driven competitive dynamics.

Key-Words: Two-species Chemotaxis models, Competitive Interspecies, Asymptotic behaviour, Volume-filling effects, Weighted networks, Exponential and algebraic decay.

Received: March 26, 2025. Revised: August 8, 2025. Accepted: August 26, 2025. Published: May 12, 2026.

1 Introduction

The study of long-time behavior in reaction-diffusion systems, particularly those involving chemotaxis and interspecies competition, has gained significant attention due to its relevance in modeling complex biological and ecological processes. Traditional analysis in continuous Euclidean domains has been extended in recent years to networked structures, which naturally represent environments with spatial heterogeneity, directionality, and connectivity constraints, such as neural, vascular, or ecological transport networks.

In such settings, the underlying network topology and edge weights play a crucial role in shaping the dynamics of the system. A weighted network is a graph where edges are endowed with weights that influence diffusion and transmission rates of the interacting species or chemical signals. These weights introduce anisotropy and inhomogeneity in space, resulting in behavior that may diverge significantly from that observed in standard domains.

Understanding the long-time behavior of solutions on weighted networks involves examining whether solutions converge to steady states, decay, or exhibit more complex dynamics such as oscillations or segregation. Of particular interest is the stability of equilibrium states under various interaction regimes, for instance, weak versus strong interspecies competition. From a modeling perspective, the competition mechanisms considered here extend classical LotkaVolterra interactions, [1], [2], to structured spatial networks, complementing recent generalizations, [3], [4].

Next, a threshold condition, necessary to prevent overcrowding, has a clear biological interpretation that was introduced in [5], and is known as the ”volume-filling effect”. The presence of this effect, where movement becomes restricted as densities approach a saturation threshold, further complicates the analysis by introducing nonlinear degeneracies in the diffusion and chemotactic terms.

In two-species chemotactic systems, long-time analysis typically involves constructing appropriate Lyapunov functionals to capture the system's energy dissipation properties. These functionals allow one to prove exponential or algebraic convergence toward equilibrium, depending on the strength of the interaction parameters. Moreover, the network structure affects the speed and nature of convergence: nodes with high connectivity or large edge weights can accelerate propagation or segregation phenomena, while bottlenecks may delay or alter stabilization. Moreover, numerical simulations have proven interesting biological dynamics in multi-species models as in continuous domains.

This work generalizes the numerical study into dynamics in networked environments.

The qualitative behavior of multi-species chemotaxis systems, including global existence, finite-time blow-up, and asymptotic stability, has been extensively investigated in continuous domains, [6], [7], [8], [9], [10], [11], [12], [13]. At the same time, robust and energy-stable numerical schemes have been developed in recent years, [14], [15], [16]. The analysis of such systems on networks requires the adaptation of classical PDE tools, such as compactness arguments, entropy estimates, and Sobolev embeddings, to graph-based function spaces. Recent advances in PDE analysis on graphs have highlighted the role of unbounded Laplacians and network topology in determining long-time dynamics, [17], [18]. A central challenge lies in handling the Kirchhoff-type transmission conditions at the nodes, which ensure conservation across network junctions.

In this context, the present work contributes to the growing body of research on network-based PDEs by rigorously analyzing the asymptotic behavior of a two-species chemotaxis-competition system with degenerate volume-filling mechanisms on weighted networks. The results reveal how the interplay between nonlinearity, competition strength, and network geometry determines the eventual fate of the species involved, whether coexistence, extinction, or spatial segregation, and provide both theoretical guarantees and numerical evidence supporting these outcomes.

For that, we analyze the following generalized competing two-species chemotaxis model:

$$\begin{cases} \partial_t U - \Delta U + \nabla \cdot \Big(\chi_1(U)\nabla V\Big) \\ = \mu_1 U(1-U-\alpha_1 W), \\ \\ \partial_t W - \Delta W + \nabla \cdot \Big(\chi_2(W)\nabla V\Big) \\ = \mu_2 W(1-W-\alpha_2 U), \\ \\ \partial_t V - \Delta V = -(\alpha U + \beta W)V,\ t>0,\ y \in \Omega \end{cases} \tag{1}$$

where Ω is an open bounded domain. The system is supplemented by the following boundary conditions on $\partial\Omega \times (0,T)$,

$$\nabla U \cdot \eta = 0,\ \nabla W \cdot \eta = 0,\ \nabla V \cdot \eta = 0, \tag{2}$$

where η is the exterior unit normal to $\partial\Omega$. The initial conditions on Ω are given by,

$$U(x,0) = U_0(x), W(x,0) = W_0(x), \tag{3}$$
$$V(x,0) = V_0(x)\,.$$

The details regarding all the variables of system (1) are provided in Table 1.

Table 1: Variables description. Source: created by the author.

Variables	Description
U, W	The density of species 1 and 2
V	The concentration of the chemical
$\chi_1(U)$, $\chi_2(W)$	The chemotactic sensitivity functions
μ_1, $\mu_2 > 0$	The growth rate of populations 1 and 2
α_1, $\alpha_2 > 0$	The strength of populations 1 and 2 in competition
α, $\beta > 0$	The consumption rate of chemicals by populations 1 and 2

Nonlinear and degenerate chemotactic sensitivities χ_1 and χ_2 approach zero as the population densities U and W are close to 0 or a normalized density 1. Hence, we suppose initially that $\chi_1(0) = \chi_2(0) = 0$ and that the chemotactic sensitivities χ_1 and χ_2 vanish when $U \geq 1$ and $W \geq 1$.

2 Problem Setting

This section outlines the main assumptions and mathematical framework necessary to ensure mathematical well-posedness, proved similarly as in [19], of the proposed chemotaxis-competition model on networks.

2.1 Assumptions and Initial Data

To accurately reflect biologically constrained environments, we impose the following assumptions on the chemotactic sensitivity functions:

$$\text{The functions } \chi_1,\, \chi_2 \text{ belong to the set} \tag{4}$$
$$\{w \in C([0,1], \mathbb{R}^+) \text{ such that } w(0) = w(1) = 0\}\,.$$

This ensures that the chemotactic response vanishes both in the absence of individuals and under crowding conditions.

The initial data are assumed to satisfy the bounds:

$$0 \leq U_0 \leq 1,\ 0 \leq W_0 \leq 1, V_0 \geq 0 \text{ a.e. in } \Omega \tag{5}$$

and $V_0 \in L^\infty(\Omega)$.

2.2 Weighted network Structure

Before formally stating the model on the network Γ, we introduce the necessary notation and definitions for the graph structure and function spaces. Let $\Gamma = (\mathcal{V}, \mathcal{E})$ be a finite, connected, undirected graph, where:

- $\mathcal{V} = \{v_1, \cdots, v_n\}$ is the set of n vertices (nodes),
- $\mathcal{E} = \{e_1, \cdots, e_m\}$ is the set of m edges, each associated with a finite, open interval.

Each edge $e_i \in \mathcal{E}$ is normalized to the interval $[0,1]$ and admits two orientations, denoted $\overline{e_i}^{\pm}$. For each oriented edge, we define homeomorphisms:

$$h_i^{\pm} : [0,1] \to \overline{e_i}^{\pm} \text{ such that } h_i^+(0) = h_i^-(1) \text{ and}$$
$$h_i^+(1) = h_i^-(0).$$

An arc a_i corresponds to an oriented edge, and we denote:

- $I(a_i)$: initial node of a_i,
- $T(a_i)$: terminal node of a_i,
- $-a_i$: arc in the opposite orientation.

For any vertex $v_i \in \mathcal{V}$, define the local edge set:

$$E(v_i) = \{e_i \in \mathcal{E},\ v_i \text{ is an endpoint of } e_i\}, \text{ with}$$
$$d(v_i) = |E(v_i)|,$$

where $d(v_i)$ is the degree of the node v_i.

A path C of length k as a sequence $(a_{i_1}, \cdots, a_{i_k})$ of arcs such that $T(a_{i_l}) = I(a_{i_{l+1}})$, $l = 1, \cdots, k-1$. Denote by $|C|$ the length of the path C and by $C_k(x,y)$ the set of all paths of length k with $x \in a_{i_1}$, $y \in a_{i_k}$.

For points $x, y \in \overline{e_i}$, we define the distance along the edge as:

$$d(x,y) := \left| (h_i^{\pm})^{-1}(x) - (h_i^{\pm})^{-1}(y) \right|.$$

Then, the distance along a path $C \in C_k(x,y)$ is given by:

$$d_C(x,y) := d(x, T(a_{i_1})) + d(y, I(a_{i_k})) + |C| - 2.$$

Each edge $e_i \in \mathcal{E}$ is assigned a positive weight $\kappa(e_i)$ satisfying:

$$0 < \kappa_0 \le \kappa(e_i) \le \kappa_1,\ \forall i = 1, \cdots, m.$$

The transfer/reflection coefficient from the arc a_i to the arc a_j is defined as:

$$\varepsilon_{(a_i \to a_j)} := \begin{cases} 2\kappa(e_i)\Big(\displaystyle\sum_{l \in E(T(a_i))} \kappa(e_l)\Big)^{-1} & \text{if } a_j \neq -a_i \\ & \text{(transmission)} \\ 2\kappa(e_i)\Big(\displaystyle\sum_{l \in E(T(a_i))} \kappa(e_l)\Big)^{-1} - 1 & \text{if } a_j = -a_i \\ & \text{(reflection)} \\ 0 & \text{otherwise}. \end{cases} \tag{6}$$

These coefficients determine how densities are transmitted or reflected at graph junctions. The weight of a path $C = (a_{i_1}, \cdots, a_{i_k})$ is given by :

$$\varepsilon(C) := \prod_{l=1}^{k-1} \varepsilon_{(a_{i_l} \to a_{i_{l+1}})}. \tag{7}$$

2.3 Function spaces on the network

We now define the appropriate functional framework for the analysis of evolution equations on the network Γ. A function $u : \Gamma \to \mathbb{R}$ is represented as a collection $u = (u_i)_{i=1}^m$, with each component u_i defined on the normalized edge $\overline{e_i}$ of length 1. For any $y \in e_i$, set $\xi = (\pi_i^{\pm})^{-1}(y) \in [0,1]$, so that:

$$u_i(y) = \tilde{u}_i(\xi), \text{ where } \tilde{u}_i = u \circ \pi_i^{\pm}.$$

The integral of u over the graph is defined as:

$$\int_\Gamma u(y)\, dy := \sum_{i=1}^m \kappa(e_i) \int_0^1 \tilde{u}_i(\xi)\, d\xi.$$

The space of square-integrable functions on Γ is:

$$L^2(\Gamma) := \{u = (u_i)_{i=1}^m;\ u_i \in L^2(e_i)\}$$
$$= \{u;\ ||u||^2_{L^2(\Gamma)} = \sum_{i=1}^m \kappa(e_i) ||\tilde{u}_i||^2_{L^2(0,1)} < +\infty\},$$

with scalar product

$$< u, w >_\Gamma = \sum_{i=1}^m \kappa(e_i) \int_0^1 \tilde{u}_i(\xi) \tilde{w}_i(\xi)\, d\xi,$$

and associated norm $||u||^2_{L^2(\Gamma)} = < u, u >_\Gamma$.

More generally, we define:

$$L^p(\Gamma) = \{u;\ ||u||^p_{L^p} = \sum_{i=1}^m \kappa(e_i) ||\tilde{u}_i||^p_{L^p(0,1)} < \infty\},$$

$$L^\infty(\Gamma) = \{u;\ ||u||_{L^\infty(\Gamma)} =$$

$$\max_{i=1,\cdots,m} \kappa(e_i)||\tilde{u}_i||_{L^\infty(0,1)} < \infty\}\,.$$

We also define the space of continuous functions on the network:

$$C^0(\Gamma) = \{u = (u_i)_{i=1}^m;$$

$$u_i(v_j) = u_k(v_j),\ i,k \in E(v_j),\ j = 1,\cdots,n\}\,,$$

and the Sobolev spaces:

$$H^1(\Gamma) = \{u \in L^2(\Gamma),\ \partial_y u_i \in L^2(\Gamma)$$

$$\text{and } u_i(v_j) = u_k(v_j),\ i,k \in E(v_j),\ j = 1,\cdots,n\}\,,$$

$$\forall 1 \le r < +\infty,\ H^r(\Gamma) = \{u \in C^0(\Gamma),$$

$$||u||^2_{H^r(\Gamma)} = \sum_{i=1}^m \kappa(e_i)||\tilde{u}_i||^2_{H^r(0,1)} < +\infty\}\,,$$

$$W^{1,\infty}(\Gamma) = \{u \in C^0(\Gamma),\ u' \in L^\infty(\Gamma)\}\,.$$

Finally, we denote by $(H^1(\Gamma))'$ the dual of $H^1(\Gamma)$ consisting of continuous linear functionals. A standard compactness result holds: $L^2(0,T;H^1(\Gamma)) \cap H^1(0,T;(H^1(\Gamma))')$ into $C(0,T;L^2(\Gamma))$, is continuous, with the embedding being continuous, as can be shown using techniques similar to those employed for PDEs on standard intervals.

2.4 Discrete Interspecies Model

We now present the interspecies competition model incorporating volume-filling effects and nonlinear degenerate convective fluxes on a network Γ. For all $t > 0$, $y \in \Gamma$, $i = 1,\cdots,m$ and $j = 1,\cdots,n$, the system reads:

$$\begin{cases} \partial_t U_i = \partial_{yy} U_i - \partial_y (U_i(1-U_i)\partial_y V_i) \\ +\mu_1 U_i(1 - U_i - \alpha_1 W_i),\ \text{on } [0,+\infty[\times e_i, \\ \\ \partial_t W_i = \partial_{yy} W_i - \partial_y (W_i(1-W_i)\partial_y V_i) \\ +\mu_2 W_i(1 - W_i - \alpha_2 U_i),\ \text{on } [0,+\infty[\times e_i, \\ \\ \partial_t V_i = \partial_{yy} V_i - (\alpha U_i + \beta W_i) V_i \\ \text{on } [0,+\infty[\times e_i, \end{cases} \tag{8}$$

$$\begin{cases} U_i(0,y) = U_i^0(y), W_i(0,y) = W_i^0(y), \\ V_i(0,y) = V_i^0(y) \text{ (initial conditions)} \\ \\ U_i(t,v_j) = U_k(t,v_j), W_i(t,v_j) = W_k(t,v_j) \\ V_i(t,v_j) = V_k(t,v_j) \text{ if } i,k \in E(v_j) \text{ (continuity)} \\ \\ \displaystyle\sum_{i\in E(v_j)} \kappa(e_i)\Big(\frac{\partial U_i}{\partial n}(t,v_j) - U_i(t,v_j)(1-U_i(t,v_j)) \\ \frac{\partial V_i}{\partial n}(t,v_j)\Big) = 0, \\ \\ \displaystyle\sum_{i\in E(v_j)} \kappa(e_i)\Big(\frac{\partial W_i}{\partial n}(t,v_j) - W_i(t,v_j)(1-W_i(t,v_j)) \\ \frac{\partial V_i}{\partial n}(t,v_j)\Big) = 0, \\ \\ \displaystyle\sum_{i\in E(v_j)} \kappa(e_i)\frac{\partial V_i}{\partial n}(t,v_j) = 0 \text{ (transmission).} \end{cases} \tag{9}$$

This system (8) governs the dynamics of species U and W, as well as the chemical signal V, across the network composed of m edges. The conservation of flux at the nodes is rigorously enforced in (9) through the continuity and Kirchhoff-type conditions.

3 Asymptotic behavior

This section analyzes the long-term behavior of our system (8) using Lyapunov functionals and proves the convergence of the solutions toward equilibrium states under two main scenarios.

Theorem 3.1. *(Asymptotic behavior) Let $(U_0, W_0, V_0) \in \mathcal{U}$ satisfying* (5)*. Then,*

- *the chemical concentration $V(t)$ decays exponentially to zero as $t \to +\infty$.*
- *In the strict extinction regime $\alpha_1 = 1 > \alpha_2$, the solution $(U(t), W(t))$ converges algebraically towards $(0,1)$; for some $C, t_1 > 0$, $||U||_{L^1(\Gamma)} + ||W-1||^2_{L^2(\Gamma)} \le \frac{C}{t+t_1}$ for some $C, t_1 > 0$.*
- *In all other cases, the solution $(U(t), W(t))$ converges exponentially to the steady state $(\overline{U}, \overline{W})$ in $L^2(\Gamma)$.*

Proof. Let us start by the case of $\alpha_1, \alpha_2 \in (0,1)$ and of strictly positive steady states $\overline{U}, \overline{W}$. For that, we define the classical entropy functional:

$$E_1 = \int_\Gamma (U - \overline{U} - \overline{U}\log\Big(\frac{U}{\overline{U}}\Big))dy +$$

$$\lambda_1 \int_\Gamma (W - \overline{W} - \overline{W}\log\Big(\frac{W}{\overline{W}}\Big))dy + \frac{l_1}{2}\int_\Gamma V^2 dy$$
$$= \theta_1(t) + \lambda_1\theta_2(t) + l_1\theta_3(t)\,.$$

Notice that:

$$\theta_1(t) = \int_\Gamma (U - \overline{U}\log(U)) - (\overline{U} - \overline{U}\log(\overline{U}))\,dy$$
$$= \int_\Gamma \Big(\mathcal{H}(U) - \mathcal{H}(\overline{U})\Big)\,dy\,,$$

where $\mathcal{H}(s) = s - \overline{U}\,log(s)$ for $s > 0$, $\mathcal{H}'(\overline{U}) = 0$ and $\mathcal{H}(U) - \mathcal{H}(\overline{U}) = \frac{\mathcal{H}''(\xi)}{2}(U-\overline{U})^2 = \frac{\overline{U}}{2\xi^2}(U-\overline{U})^2$ hence $\theta_1(t) \geq 0$ due to Taylor Formula.

The derivative of the functional is given as:

$$\frac{d\,E_1}{dt} = \int_\Gamma (1 - \frac{\overline{U}}{U})\frac{dU}{dt}\,dy + \lambda_1\int_\Gamma (1 - \frac{\overline{W}}{W})\frac{dW}{dt}\,dy$$
$$+ l_1\int_\Gamma V\frac{dV}{dt}\,dy$$
$$= \sum_{i=1}^m \kappa(e_i)\Big[\int_0^1 (1 - \frac{\overline{\tilde{U}_i}}{\tilde{U}i})\partial_t\tilde{U}_i(t,\eta)d\eta$$
$$+ \lambda_1\int_0^1 (1 - \frac{\overline{\tilde{W}_i}}{\tilde{W}i})\partial_t\tilde{W}_i(t,\eta)d\eta$$
$$+ l_1\int_0^1 \tilde{V}_i\partial_t\tilde{V}_i(t,\eta)d\eta\Big]$$
$$= \sum_{i=1}^m \kappa(e_i)\Big[\int_0^1 (1 - \frac{\overline{\tilde{U}_i}}{\tilde{U}_i})\partial_{\eta\eta}U\,d\eta$$
$$- \int_0^1 (1 - \frac{\overline{\tilde{U}_i}}{\tilde{U}_i})\partial_\eta(\chi_1(\tilde{U}_i)\partial_\eta\tilde{V}_i)\,d\eta$$
$$+ \mu_1\int_0^1 (1 - \frac{\overline{\tilde{U}_i}}{\tilde{U}_i})\tilde{U}_i(1 - \tilde{U}_i - \alpha_1\tilde{W}_i)\,d\eta$$
$$+ \lambda_1\int_0^1 (1 - \frac{\overline{\tilde{W}_i}}{\tilde{W}_i})\partial_{\eta\eta}W\,d\eta$$
$$- \lambda_1\int_0^1 (1 - \frac{\overline{\tilde{W}_i}}{\tilde{U}_i})\partial_\eta(\chi_2(\tilde{W}_i)\partial_\eta\tilde{V}_i)\,d\eta$$
$$+ \mu_2\lambda_1\int_0^1 (1 - \frac{\overline{\tilde{W}_i}}{\tilde{W}_i})\tilde{W}_i(1 - \tilde{W}_i - \alpha_2\tilde{U}_i)\,d\eta$$
$$+ l_1\int_0^1 \tilde{V}_i\partial_{\eta\eta}\tilde{V}_i\,d\eta - l_1\int_0^1 \tilde{V}_i^2(\alpha\tilde{U}_i + \beta\tilde{W}_i)\,d\eta\Big]\,.$$

Using that

$$\mu_1\int_0^1 (1 - \frac{\overline{\tilde{U}_i}}{\tilde{U}_i})\tilde{U}_i(1 - \tilde{U}_i - \alpha_1\tilde{W}_i) = \mu_1\int_0^1 (\tilde{U}_i - \overline{\tilde{U}_i})$$
$$- \mu_1\int_0^1 \overline{\tilde{U}_i}(\tilde{U}_i - \overline{\tilde{U}_i}) - \alpha_1\mu_1\int_0^1 (\tilde{U}_i - \overline{\tilde{U}_i})\overline{\tilde{W}_i}$$
$$- \mu_1\int_0^1 (\tilde{U}_i - \overline{\tilde{U}_i})^2 - \alpha_1\mu_1\int_0^1 (\tilde{U}_i - \overline{\tilde{U}_i})(\tilde{W}_i - \overline{\tilde{W}_i})$$

and since $(\overline{\tilde{U}_i}, \overline{\tilde{W}_i})$ is an equilibrium solution then:

$$\frac{d\,E_1}{dt} = \sum_{i=1}^m \kappa(e_i)\Big[-\overline{\tilde{U}_i}\int_0^1 \frac{|\partial_\eta\tilde{U}_i|^2}{\tilde{U}_i^2}\,d\eta$$
$$+ \overline{\tilde{U}_i}\int_0^1 \frac{1 - \tilde{U}_i}{\tilde{U}_i}\partial_\eta\tilde{U}_i\partial_\eta\tilde{V}_i\,d\eta$$
$$- \mu_1\int_0^1 (\tilde{U}_i - \overline{\tilde{U}_i})^2\,d\eta - \alpha_1\mu_1\int_0^1 (\tilde{U}_i - \overline{\tilde{U}_i})(\tilde{W}_i - \overline{\tilde{W}_i})\,d\eta$$
$$- \lambda_1\overline{\tilde{W}_i}\int_0^1 \frac{|\partial_\eta\tilde{W}_i|^2}{\tilde{W}_i^2}\,d\eta + \lambda_1\overline{\tilde{W}_i}\int_0^1 \frac{1 - \tilde{W}_i}{\tilde{W}_i}\partial_\eta\tilde{W}_i\partial_\eta\tilde{V}_i\,d\eta$$
$$- \mu_1\lambda_1\int_0^1 (\tilde{W}_i - \overline{\tilde{W}_i})^2\,d\eta$$
$$- \alpha_2\mu_2\lambda_1\int_0^1 (\tilde{U}_i - \overline{\tilde{U}_i})(\tilde{W}_i - \overline{\tilde{W}_i})\,d\eta$$
$$- l_1\int_0^1 |\partial_\eta\tilde{V}_i|^2\,d\eta - l_1\int_0^1 \tilde{V}_i^2(\alpha\tilde{U}_i + \beta\tilde{W}_i)\,d\eta\Big]\,.$$

Therefore, using that $\tilde{U}_i \leq 1$, $\tilde{W}_i \leq 1$, Young inequality and the positivity of the last integral:

$$\frac{d\,E_1}{dt} \leq \sum_{i=1}^m \kappa(e_i)\Big[-\frac{\overline{\tilde{U}_i}}{2}\int_0^1 \frac{|\partial_\eta\tilde{U}_i|^2}{\tilde{U}_i^2}\,d\eta$$
$$- \frac{\overline{\tilde{W}_i}}{2}\int_0^1 \frac{|\partial_\eta\tilde{W}_i|^2}{\tilde{W}_i^2}\,d\eta$$
$$+ (\frac{\overline{\tilde{U}_i}}{2} + \lambda_1\frac{\overline{\tilde{W}_i}}{2} - l_1)\int_0^1 |\partial_\eta\tilde{V}_i|^2\,d\eta$$
$$- \mu_1\int_0^1 (\tilde{U}_i - \overline{\tilde{U}_i})^2\,d\eta - \mu_1\lambda_1\int_0^1 (\tilde{W}_i - \overline{\tilde{W}_i})^2\,d\eta$$
$$- (\alpha_1\mu_1 + \alpha_2\mu_2\lambda_1)\int_0^1 (\tilde{U}_i - \overline{\tilde{U}_i})(\tilde{W}_i - \overline{\tilde{W}_i})\,d\eta\Big]\,.$$

To prove the negativity of the derivative of the entropy function, we must deal with the last term in the previous inequality. Hence, we can choose $\lambda_1 = \frac{\alpha_1\mu_1}{\alpha_2\mu_2} > 0$ to obtain:

$$- \mu_1\int_0^1 (\tilde{U}_i - \overline{\tilde{U}_i})^2\,d\eta - \mu_1\lambda_1\int_0^1 (\tilde{W}_i - \overline{\tilde{W}_i})^2\,d\eta$$
$$- (\alpha_1\mu_1 + \alpha_2\mu_2\lambda_1)\int_0^1 (\tilde{U}_i - \overline{\tilde{U}_i})(\tilde{W}_i - \overline{\tilde{W}_i})\,d\eta$$
$$\leq -\varepsilon_1\int_0^1 (\tilde{U}_i - \overline{\tilde{U}_i})^2\,d\eta$$

$$-\Big(\frac{\alpha_1\mu_1}{\alpha_2}-\frac{4\alpha_1^2\mu_1^2}{4(\mu_1-\varepsilon_1)}\Big)\int_0^1(\tilde{W}_i-\overline{\tilde{W}_i})^2\,d\eta\,.$$

It is sufficient to choose $0<\varepsilon_1<\mu_1(1-\alpha_1\alpha_2)<\mu_1$ in our case. Consequently and for $l_1>\frac{\overline{\tilde{U}_i}}{2}+\lambda_1\frac{\overline{\tilde{W}_i}}{2}>0$, one has:

$$\frac{d\,E_1}{dt}\le\sum_{i=1}^m\kappa(e_i)\Big[-\varepsilon_1\int_0^1(\tilde{U}_i-\overline{\tilde{U}_i})^2\,d\eta$$
$$-\alpha_1\mu_1\Big(\frac{1}{\alpha_2}-\frac{\alpha_1\mu_1}{\mu_1-\varepsilon_1}\Big)\int_0^1(\tilde{W}_i-\overline{\tilde{W}_i})^2\,d\eta\Big]$$
$$\le-\sigma_1\Big(||U-\overline{U}||^2_{L^2(\Gamma)}+||W-\overline{W}||^2_{L^2(\Gamma)}\Big)\,,$$

where $\sigma_1=\min(\varepsilon_1,\alpha_1\mu_1\Big(\frac{1}{\alpha_2}-\frac{\alpha_1\mu_1}{\mu_1-\varepsilon_1}\Big))>0$.

Next, we integrate with respect to t, then:

$$\int_0^{+\infty}\Big(||U-\overline{U}||^2_{L^2(\Gamma)}+||W-\overline{W}||^2_{L^2(\Gamma)}\Big)$$
$$\le\frac{E_1(0)-E_1(\infty)}{\sigma}\,.$$

As we have, E_1 is positive and decreasing then $E_1(\infty)\ge0$. Hence,

$$\int_0^{+\infty}\Big(||U-\overline{U}||^2_{L^2(\Gamma)}+||W-\overline{W}||^2_{L^2(\Gamma)}\Big)<\infty\,.$$

Using a classical Lemma of Barbalat, one has

$$||U-\overline{U}||^2_{L^2(\Gamma)}+||W-\overline{W}||^2_{L^2(\Gamma)}\to0,\ \text{as } t\to+\infty\,.$$

We turn now into the second case $\alpha_1=1>\alpha_2$ where $\overline{U}=0$ and $\overline{W}=1$. For that, we define the following classical entropy functional:

$$E_2=\int_\Gamma U\,dy+\lambda_2\int_\Gamma(W-1-\log(W))dy$$
$$+\frac{l_2}{2}\int_\Gamma V^2dy=\sum_{i=1}^m\kappa(e_i)\Big[\int_0^1\tilde{U}_i\,d\eta$$
$$+\lambda_2\int_0^1(\tilde{W}_i-1-\log(\tilde{W}_i))d\eta+\frac{l_2}{2}\int_0^1\tilde{V}_i^2d\eta\Big]$$
$$=\theta_1(t)+\lambda_2\theta_2(t)+l_2\theta_3(t)\,.$$

Therefore using the same guidelines and that $-\alpha_1\le-1$, one has

$$\frac{d\,E_2}{dt}=\sum_{i=1}^m\kappa(e_i)\Big[\int_0^1\partial_t\tilde{U}_i\,d\eta$$
$$+\lambda_2\int_0^1(1-\frac{1}{\tilde{W}_i})\partial_t\tilde{W}_i\,d\eta+l_2\int_0^1\tilde{V}_i\partial_t\tilde{V}_i\,d\eta\Big]$$
$$\le\sum_{i=1}^m\kappa(e_i)\Big[-\mu_1\int_0^1\tilde{U}_i^2\,d\eta$$
$$-(\mu_1+\lambda_2\alpha_2\mu_2)\int_0^1\tilde{U}_i(\tilde{W}_i-1)\,d\eta$$
$$-\lambda_2\mu_2\int_0^1(\tilde{W}_i-1)^2\,d\eta+(\frac{\lambda_2}{2}-l_2)\int_0^1|\partial_\eta\tilde{V}_i|^2\,d\eta\Big]\,.$$

Take $\lambda_2=\frac{\mu_1}{\alpha_2\mu_2}>0$, $0<\varepsilon_2<\mu_1(1-\alpha_2)<\mu_1$ and $l_2>\frac{\lambda_2}{2}$ to obtain:

$$\frac{d\,E_2}{dt}\le-\varepsilon_2\int_\Gamma U^2\,d\eta$$
$$-\Big(\frac{\mu_1}{\alpha_2}-\frac{\mu_1^2}{\mu_1-\varepsilon_2}\Big)\int_\Gamma(W-1)^2\,d\eta$$
$$\le-\sigma_2\Big(||U||^2_{L^2(\Gamma)}+||W-1||^2_{L^2(\Gamma)}\Big)\,,$$

where $\sigma_2=\min(\varepsilon_2,\mu_1\Big(\frac{1}{\alpha_2}-\frac{\mu_1}{\mu_1-\varepsilon_2}\Big))>0$. Consequently,

$$||U||^2_{L^2(\Gamma)}+||W-1||^2_{L^2(\Gamma)}\to0,\ \text{as } t\to+\infty\,.$$

Exponential decay of V. We fix $t_0>1$;

$$\frac12\frac{d}{dt}||V||^2_{L^2(\Gamma)}\le-\frac{\alpha\overline{U}+\beta\overline{W}}{2}||V||^2_{L^2(\Gamma)}\,,$$

because the convergence implies

$$\frac{\overline{U}}{2}\le U\le\frac{3\overline{U}}{2}\ \text{and}\ \frac{\overline{W}}{2}\le W\le\frac{3\overline{W}}{2}\,. \tag{10}$$

Thus,

$$||V||^2_{L^2(\Gamma)}\le||V_0||^2_{L^2(\Gamma)}e^{-(\alpha\overline{U}+\beta\overline{W})t},\ \forall t\ge t_0\,.$$

Then, we can easily deduce that, in all cases, $V\to0$, as $t\to+\infty$. Moreover, we can say that V stabilizes to zero exponentially.

Exponential decay of U and W in the case α_1 and α_2 in $(0,1)$. For $U\le\xi\le\overline{U}$ and using (10), we have:

$$\frac{1}{2\overline{U}}\int_\Gamma(U-\overline{U})^2\,dy\le\int_\Gamma\Big(\mathcal{H}(U)-\mathcal{H}(\overline{U})\Big)\,dy$$
$$=\int_\Gamma\frac{\overline{U}}{2\xi^2}(U-\overline{U})^2\,dy\le\frac{2}{\overline{U}}\int_\Gamma(U-\overline{U})^2\,dy\,.$$

Then,

$$\frac{dE_1}{dt}\le-\sigma_1F_1\le-\sigma_1C_1E_1$$
$$+\frac{l_1}{2}\sigma_1C_1||V_0||^2_{L^2(\Gamma)}e^{-\frac{(\alpha\overline{U}+\beta\overline{W})}{2}t}\,,$$

where $C_1=\max\{\frac{2}{\overline{U}},\frac{2\lambda_1}{\overline{W}}\}>0$. Consequently, for $P=\frac{l_1}{2}\sigma_1C_1||V_0||^2_{L^2(\Gamma)}$, one has:

$$\frac{dE_1}{dt}+\sigma_1C_1E_1\le Pe^{-(\alpha\overline{U}+\beta\overline{W})t}\,.$$

The solution of the homogeneous equation is $E_1^{(1)}=Ce^{-\sigma_1C_1t}$ and the particular one for the nonhomogeneous equation is $E_1^{(2)}=\frac{P}{\sigma_1C_1-(\alpha\overline{U}+\beta\overline{W})}e^{(-(\alpha\overline{U}+\beta\overline{W}))t}$ using the variation of constant method. We need that $C_1>\frac{(\alpha\overline{U}+\beta\overline{W})}{\sigma_1}$ to ensure the positivity of $E_1^{(2)}$. Thus, the final choice is $C_1=\max\{\frac{2}{\overline{U}},\frac{2\lambda_1}{\overline{W}},\frac{(\alpha\overline{U}+\beta\overline{W})}{\sigma_1}\}>0$. Hence,

$$E_1(t)\le C_2e^{-\min\{\sigma_1C_1,\alpha\overline{U}+\beta\overline{W}\}\,t}\,,$$

where C_2 is an arbitrary positive constant. One can easily say now that U and W stabilize to $\overline{U}$ and $\overline{W}$ exponentially.

Algebraic decay of U and W in the case of $\alpha_1=1>$ α_2. In the neighborhood of 1, one has $|W-1-\log W|\le|W-1|$ since the ratio limit at 1 is zero. Then, using the Cauchy-Schwarz inequality:

$$E_2(t)\le P_1(||U||_{L^2(\Gamma)}+||W-1||_{L^2(\Gamma)})+P_2e^{-\beta t}\,,$$

with $P_1 = \max\{1, \lambda_2\}|\Gamma|^{\frac{1}{2}}$ and $P_2 = \frac{l_2}{2}||V_0||^2_{L^2(\Gamma)}$. Using that $\sqrt{a} + \sqrt{b} \leq \sqrt{2(a+b)}$, $\forall$, $a, b \geq 0$, then

$$E_2(t) \leq \sqrt{2}P_1(F_2(t))^{\frac{1}{2}} + P_2 e^{-\beta t}\,,$$

where $F_2(t) = \left(||U||^2_{L^2(\Gamma)} + ||W-1||^2_{L^2(\Gamma)}\right)$. Hence,

$$E_2^2(t) \leq 4P_1^2 F_2(t) + 2P_2^2 e^{-2\beta t}\,,$$

because $(a+b)^2 \leq 2a^2 + 2b^2$. Consequently,

$$\frac{dE_2}{dt} \leq -\sigma_2 F_2(t) \leq -\frac{\sigma_2}{4P_1^2}E_2^2(t) + \frac{\sigma_2 P_2^2}{2P_1^2}$$

which is not a linear dissipation inequality. Using (10), classical algebraic computations and ODE comparison argument as in [20], we can deduce that: $\forall t \geq t_1 \geq t_0$,

$$||U||_{L^1(\Gamma)} + ||W-1||^2_{L^2(\Gamma)} \leq E_2(t) \leq \frac{C}{t+t_1},$$

and therefore the algebraic polynomial convergence of (U, W) towards $(0, 1)$.

$\square$

Corollary 3.2. *The $L^2(\Gamma)$ solution's decay established in the previous Theorem implies the corresponding $L^\infty(\Gamma)$ solution's decay.*

Proof. This result is a straightforward result from the following embedding inequalities on a finite metric graph Γ:

$$||U||_{L^\infty(\Gamma)} \leq \varepsilon||\partial_x U||_{L^2(\Gamma)} + (C_G + \frac{4C_G^3}{27\varepsilon^2})||U||_{L^1(\Gamma)}$$

and

$$||U||_{L^\infty(\Gamma)} \leq \varepsilon||\partial_x U||_{L^2(\Gamma)} + C_G(1+\frac{1}{\varepsilon})||U||_{L^2(\Gamma)},$$

where C_G is a constant depending on the graph. $\square$

4 Numerical simulations and error analysis

This section introduces many numerical simulations, performed on FORTRAN, that highlight the impact of the competition parameters, the network structure, and the nonlinear chemotactic sensitivities on the species' distribution over time. Moreover, we measure and visualize the accuracy of our numerical scheme via relative error decay in various norms.

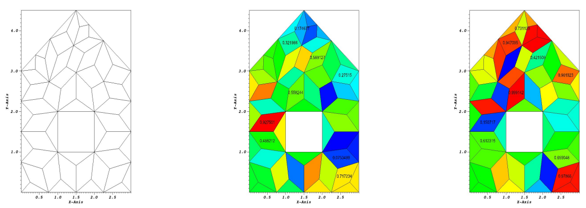

Fig. 1: Mesh (a) Initial conditions (b,c). Source: created by the author.

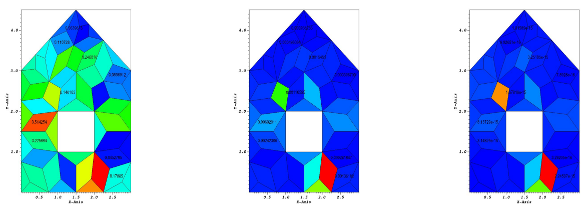

Fig. 2: Time evolution of the density of species U in the competition regime. Source: created by the author.

4.1 Simulation Setup

The competition parameters are chosen in accordance with the thresholds identified in Theorem 3.1. In particular, values satisfying $\alpha_1 \geq 1 > \alpha_2$ are used to illustrate the extinction regime, while $\alpha_1, \alpha_2 \in (0, 1)$ correspond to the coexistence regime predicted analytically.

Initial conditions for species densities $U(x, 0)$, $W(x, 0)$ are randomly introduced. The system is solved numerically with a time discretization step $\Delta t = 0.0005$ and coefficients $\alpha = 0.06$, $\beta = 0.08$, $\mu_1 = \mu_2 = 1$. Figure 1 displays the network Γ with 56 edges and the random initial distribution of the species. The numerical method is based on a recent combined finite volume-nonconforming finite element (FV-NCFE) discretization, which preserves the positivity of the solution and ensures the stability of the scheme.

4.2 Time Evolution and Dynamics

Figure 2, Figure 3 show the evolution of species densities in the strong-competition regime. One observes the extinction of species U and the dominance of W, in agreement with the theoretical convergence to the extinction state $(U, W) = (0, 1)$. Figure 4 shows, for the coexistence regime, both species persist and stabilize toward steady profiles. The simulations capture this steady coexistence, corroborating the analytical prediction of exponential convergence to an equilibrium.

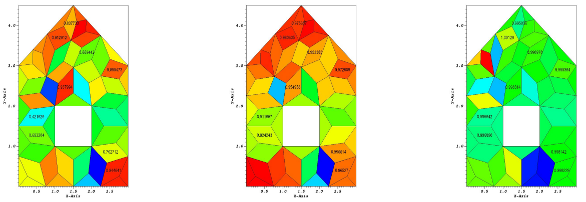

Fig. 3: Time evolution of the density of species W in the competition regime. Source: created by the author.

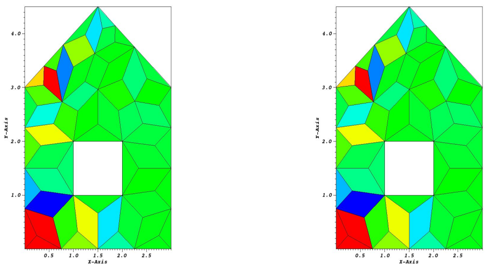

Fig. 4: Spatial distribution of the densities of species U (left) and W (right) at time $t = 4$s in the coexistence regime. Source: created by the author.

4.3 Relative Error Decay

To assess the accuracy and convergence of our numerical solver, we compute the relative errors in both $L^2(\Gamma)$ and $L^\infty(\Gamma)$ norms for the densities U, W, and the chemical concentration V. Figure 5, Figure 6 illustrate the temporal evolution of the relative L^2-errors for both species, clearly displaying a decreasing curve. In Figure 7, we analyze the decay of the error across different parameter regimes. Specifically, Figure 8 shows the exponential decay of both L^2 and L^∞-errors for species U in the strong competition case. Figure 9 shows a similar behavior for species W, with errors tending to zero exponentially. Figure 10 confirms an algebraic decay of errors in the case where $\alpha_1 = 1 > \alpha_2 = 0.1$, which matches the slower convergence rate predicted analytically.

In addition to the qualitative validation of the model, the convergence behaviour of the proposed scheme is quantitatively assessed through a mesh refinement study. In the context of networks, h denotes the maximal edge subdivision length, and mesh refinement corresponds to uniformly increasing the number of segments per edge. Numerical solutions are computed on successively

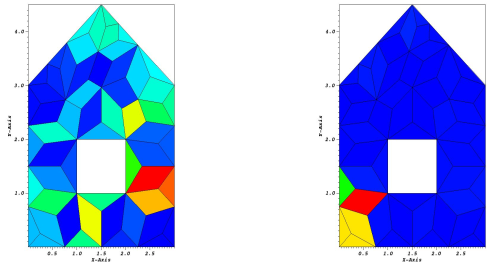

Fig. 5: Evolution in time of the L^2-relative errors for U. The edge error values are observed to decay towards zero as time increases. Source: created by the author.

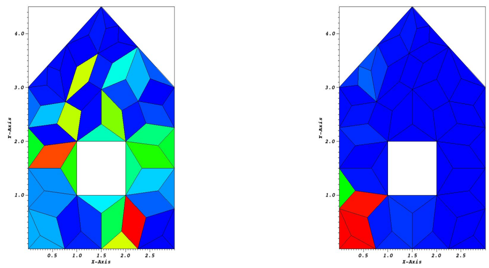

Fig. 6: Evolution in time of the L^2-relative errors for W. Source: created by the author.

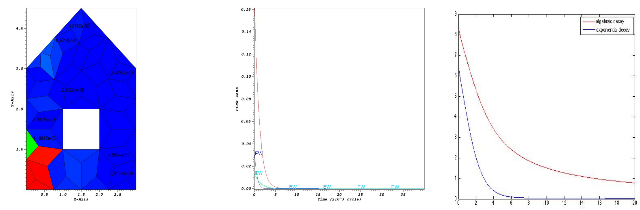

Fig. 7: Edge-wise distribution of the relative $L^2(\Gamma)$ error on the labeled network. (a), Temporal evolution of the global error functional over multiple time steps (b), Comparison between exponential and algebraic decay regimes (c). Source: created by the author.

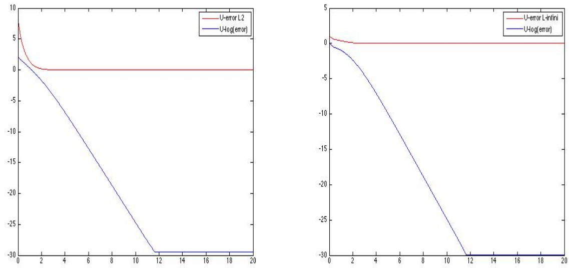

Fig. 8: Exponential decay of $L^2(\Gamma)$ and $L^\infty(\Gamma)$ errors of $||U||$ and their logs- Case $\alpha_1 = 4 > 1 > \alpha_2 = 0.1$. Source: created by the author.

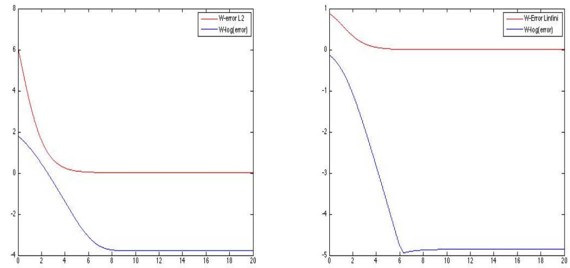

Fig. 9: Exponential decay of $L^2(\Gamma)$ and $L^\infty(\Gamma)$ errors of $||W - 1||$ and their logs- Case $\alpha_1 = 4 > 1 > \alpha_2 = 0.1$. Source: created by the author.

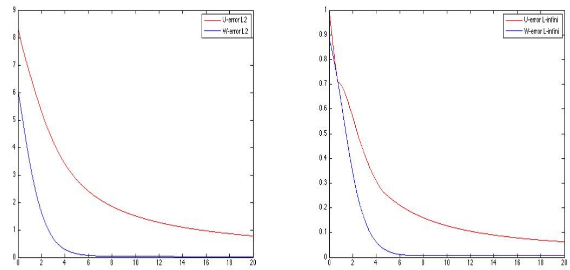

Fig. 10: Algebraic decay of $L^2(\Gamma)$ and $L^\infty(\Gamma)$ errors of $||U||$ and $||W - 1||$- Case $\alpha_1 = 1 > \alpha_2 = 0.1$. Source: created by the author.

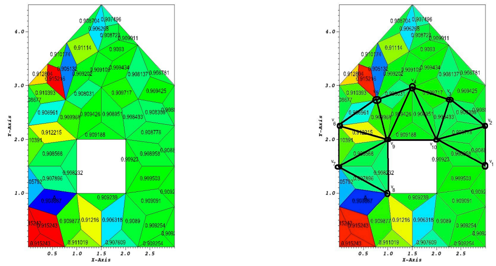

Fig. 11: (a) Labeled weighted network used in the numerical simulations. (b) Extracted subnetwork employed for the analysis of node strength influence on the stabilization behaviour. Source: created by the author.

refined discretizations $(h, \Delta t)$, $(h/2, \Delta t/2)$ and $(h/4, \Delta t/4)$. Let U_h^n denote the discrete solution at time t_n. The relative L^2-error between successive approximations is defined as $E_h(t_n) = \frac{\|U^n_{h/2} - U^n_h\|_{L^2(\Gamma)}}{\|U^n_{h/2}\|_{L^2(\Gamma)}}$. The experimental order of convergence (EOC) is then estimated by $p \approx \frac{\log(E_h/E_{h/2})}{\log(2)}$. The obtained results indicate a consistent first-order convergence rate of the scheme with respect to space and time discretization parameters.

4.4 Node Analysis and Influence

Higher node strength correlates with increased connectivity and, in some cases, with faster information or species propagation through the network. Indeed, Figure 11 shows how to label any subnetwork for the analysis of node strength. Moreover, Table 2 highlights the strengths of selected nodes in the network computed based on the aggregate edge weights.

Table 2: Strength (weighted degree) of selected nodes in the networks. Source: created by the author.

Nodes	v_1	v_5	v_{10}
Strength	1.82	2.80	4.54

To sum up, the numerical simulations strongly support the analytical predictions. These simulations not only validate the theoretical framework but also provide insights into the dynamics over complex networked domains, underscoring the role of network topology in interspecies interaction models.

4.5 Quantitative validation of entropy-based decay rates.

In the case of $\alpha_1 = 1 > \alpha_2 = 0.1$, we have proved theoretically that the entropy-based estimate predicts an algebraic decay of the form $F(t) \leq C(t+t_1)^{-1}$. To validate this convergence rate, we define the discrete error functional $F_h(t) = \|U_h(t)\|_{L^1(\Gamma)} + \|W_h(t) - 1\|^2_{L^2(\Gamma)}$ and then we extract the numerical decay order from the slope of the log-log representation. Using the data represented in Figure 10, $p_{\text{num}} = -\frac{d}{d(\log t)} \log F_h(t) \approx 1$, in agreement with the theoretical prediction.

References:

[1] A. J. Lotka, *Elements of physical biology.* Williams and Wilkins, 1925. URL: https://archive.org/details/elementsofphysic017171mbp/page/n5/mode/2up (Accessed: 01 April 2026)

[2] V. Volterra, *Variations and fluctuations of the number of individuals in animal species living together.* ICES Journal of Marine Science, Vol. 3, No. 1, 1928, pp. 3-51. DOI: https://doi.org/10.1093/icesjms/3.1.3

[3] L. Shaikhet and A. Korobeinikov, *Persistence and Stochastic Extinction in a LotkaVolterra Predator-Prey Stochastically Perturbed Model.* Mathematics, Vol. 12, No. 10, 2024, 1588. DOI: https://doi.org/10.3390/math12101588

[4] S. Samir, F. Ferraro, C. Grilletta, S. Azaele, and A. Maritan, *Generalized Lotka-Volterra Systems with Time Correlated Stochastic Interactions.* Physical Review Letters, Vol. 133, No. 16, 2024, 167101. DOI: https://doi.org/10.1103/PhysRevLett.133.167101

[5] D. Wrzosek, *Volume filling effect in modelling chemotaxis.* Mathematical Modelling of Natural Phenomena, Vol. 5, No. 1, 2010, pp. 123-147. URL: https://doi.org/10.1051/mmnp/20105106.

[6] Y. Li and Y.X. Li, *Finite-time blow-up in higher-dimensional parabolic-parabolic Chemotaxis system for two species.* Nonlinear Analysis: Theory, Methods & Applications, Vol. 109, 2014, pp. 7284. DOI: https://doi.org/10.1016/j.na.2014.05.021

[7] Q. Zhang, X. Liu, and X. Yang, *Global existence and asymptotic behavior of solutions to a two-species chemotaxis system with two chemicals.* Journal of Mathematical Physics, Vol. 58, No. 11, 2017, 111504. DOI: https://doi.org/10.1063/1.5011725

[8] C. Liu and E. Pan, *Global solutions to a two-species chemotaxis system with gradient dependent sensitivity.* Discrete and Continuous Dynamical Systems Series B, Vol. 29, No. 10, 2024, pp. 4269-4288. DOI: https://doi.org/10.3934/dcdsb.2024042

[9] D. Tran, T. Tran, and V. Tran, *On the nonlocal parabolic-elliptic Keller-Segel model in bounded domains.* Communications on Pure and Applied Analysis, Vol. 23, No. 11, 2024, pp. 1730-1747. DOI: https://doi.org/10.3934/cpaa.2024064

[10] G. Ren and B. Liu, *Global boundedness and asymptotic behavior in a two-species chemotaxis-competition system with two signals.* Nonlinear Analysis: Real World Applications, Vol. 48, 2019, pp. 288325. DOI: https://doi.org/10.1016/j.nonrwa.2019.01.017

[11] L.Wang, C. Mu, X. Hu, and P. Zheng, *Boundedness and stabilization in a two-species chemotaxis system with two chemicals.* Discrete and Continuous Dynamical Systems- B, Vol. 25, No. 1, 2020, pp. 191-221. DOI: https://doi.org/10.3934/dcdsb.2019178

[12] G. Chamoun, M. Ibrahim, M. Saad, and R. Talhouk, *Asymptotic behavior of solutions of a nonlinear degenerate chemotaxis model.* Discrete and Continuous Dynamical Systems Series B, Vol. 25, No. 11, 2020, pp. 4165-4188. DOI:https://doi.org/10.3934/dcdsb.2020092

[13] G. Li and Y. Yao, *Two-species competition model with chemotaxis: well-posedness, stability, and dynamics.* Nonlinearity, Vol 35, No. 3, 2022, pp. 1329-1359. DOI: https://doi.org/10.1088/1361-6544/ac4a8d

[14] S. Wang, S. Zhou, S. Shi, and W. Chen, *Unconditionally bound preserving and energy dissipative schemes for a class of KellerSegel equations.* SIAM Journal on Numerical Analysis, Vol. 58, No. 3, 2020, pp. 16741695. DOI: https://doi.org/10.1137/19M1246705

[15] J. Shen and J. Xu, *Fully decoupled and energy stable BDF schemes for KellerSegel*

equations. Journal of Computational Physics, Vol. 449, 2022, 110799. DOI: https://doi.org/10.1016/j.jcp.2021.110799

[16] X. Huang and J. Shein, *Efficient Numerical Schemes for a Two-Species Keller-Segel Model and Investigation of Its Blowup Phenomena in 3D.* Acta Applicandae Mathematicae, Vol. 190, No. 10, 2024. DOI:https://doi.org/10.1007/s10440-024-00647-0

[17] Y. Lin, S. Liu and Y. Wu, *Blow-up phenomenon to the semilinear heat equation for unbounded Laplacians on graphs.* Revista Matemtica Complutense, Vol. 38, No. 1, 2025, pp. 281294. DOI: https://doi.org/10.1007/s13163-024-00497-2

[18] S. Hou and X. Kong, *Existence and asymptotic behaviors of solutions to Chern-Simons systems and equations on finite graphs.* Calculus of Variations and Partial Differential Equations, Vol. 64, No. 77, 2025. DOI: https://doi.org/10.1007/s00526-025-02940-8

[19] G. Chamoun, *Mathematical analysis of parabolic models with volume-filling effect in weighted networks.* Journal of Dynamics and Differential Equations, Vol. 35, No. 3, 2023, pp. 2115-2137. DOI: https://doi.org/10.1007/s10884-021-10049-7

[20] H.-Y. Jin and T. Xiang, *Convergence rates of solutions for a two-species chemotaxis-navier-stokes system with competitive kinetics.* Discrete and continuous dynamical systems series B, Vol. 24, No. 4, 2019, pp. 1919-1942. DOI: https://doi.org/10.3934/dcdsb.2018249

Contribution of Individual Authors to the Creation of a Scientific Article (Ghostwriting Policy)

The author contributed in the present research, at all stages from the formulation of the problem to the final findings and solution.

Sources of Funding for Research Presented in a Scientific Article or Scientific Article Itself

The author gratefully acknowledges the financial support provided by Saint Joseph University of Beirut (USJ) for the completion of this research.

Conflicts of Interest

The author has no conflicts of interest to declare.

Creative Commons Attribution License 4.0 (Attribution 4.0 International, CC BY 4.0)

This article is published under the terms of the Creative Commons Attribution License 4.0
https://creativecommons.org/licenses/by/4.0/deed.en_US